RESEARCH ARTICLE

WILEY

Evolution of MEG: A first MEG-feasible fluxgate magnetometer

Nikolay Koshev[1] 🔵 | Anna Butorina[1] | Ekaterina Skidchenko[1] |
Alexey Kuzmichev[2] | Alexei Ossadtchi[3] | Maxim Ostras[2] | Maxim Fedorov[1] |
Petr Vetoshko[2,4]

[1]Skolkovo Institute of Science and Technology, Moscow, Russia

[2]M-Granat, Russian Quantum Center, Moscow, Russia

[3]Higher School of Economics, Moscow, Russia

[4]Kotelnikov Institute of Radioengineering and Electronics of RAS, Moscow, Russia

Correspondence
N. Koshev, Skolkovo Institute of Science and Technology, Bolshoy blv., 30, Moscow 121205, Russia.
Email: n.koshev@skoltech.ru

Funding information
RF Government grant, AG. No. 075-15-2021-624

Abstract
In the current article, we present the first solid-state sensor feasible for magnetoencephalography (MEG) that works at room temperature. The sensor is a fluxgate magnetometer based on yttrium-iron garnet films (YIGM). In this feasibility study, we prove the concept of usage of the YIGM in terms of MEG by registering a simple brain induced field—the human alpha rhythm. All the experiments and results are validated with usage of another kind of high-sensitive magnetometers—optically pumped magnetometer, which currently appears to be well-established in terms of MEG.

KEYWORDS
alpha rhythm, fluxgate magnetometers, magnetoencephalography, optically pumped magnetometers, yttrium-iron garnet magnetometers

1 | INTRODUCTION

Magnetoencephalography (MEG) is a unique neuroimaging modality that combines noninvasiveness with high spatial and temporal resolution. These properties place MEG among the most informative neuroimaging tools capable of localizing neuronal activity with distinct temporal structure and suitable for studying complex functional integration processes. The first demonstration of MEG in humans dates back to 1972 when Cohen (1972) used superconducting quantum interference devices (SQUIDs) to register human alpha activity. Since then MEG found numerous applications in both medicine (Boon et al., 2019; Koptelova et al., 2018; Mandal, Banerjee, Tripathi, & Sharma, 2018) and neuroscience (Baillet, 2017; da Silva, 2013; Hari & Salmelin, 2012; Pulvermüller, Shtyrov, & Ilmoniemi, 2003).

Currently, SQUID-based MEG device (SQUID-MEG) implemented in the form of a fixed-size helmet dewar remains the most widely used instrument. While SQUID-MEG has been successfully utilized in experimental and clinical neurology, the technology behind SQUID-based MEG systems limits the range of MEG advancement toward

even more exciting applications. Such systems are not only expensive but also have high maintenance costs due to the constant need for sensor cooling in the liquid helium. In addition, the application of this technique is difficult for subjects with small heads (babies, children). For adults, the distance between the sensors and the human head is about 2–3 cm (the thickness of the dewar walls) and noticeably increases for children, severely limiting the device sensitivity due to the attenuation of the magnetic field in inverse proportion to the square of the distance between the current source and the sensor (Boto et al., 2018). Despite all advantages and uniqueness of the spatial and temporal resolving properties, the mentioned technological shortcomings preclude MEG neuroimaging from widespread use. Currently, such systems are available only at several hundred locations worldwide.

Recent advances in high Tc SQUID technology allow to lift some traditional MEG systems limitations, as high Tc SQUIDS operate at liquid nitrogen temperatures which significantly minimizes operational costs and reduces requirements for dewar vessels containing the coolant. Faley et al. (2017) reviews a range of applications of this

promising technology including MEG. Nitrogen cooled SQUIDs allow to be placed significantly closer to the scalp (Andersen et al., 2017) compared to the conventional low-temperature sensors and register the activity of cortical sources with higher SNR. Proximal position also provides access to the higher spatial frequency components of the magnetic field (Andersen et al., 2020). Despite the recent progress, these sensors remain bulky as they still require cooling to liquid nitrogen temperatures implemented via 1–1.5 L cryostat.

Recent technological developments in the field of atomic magnetometry hold the promise of lifting several limitations inherent to the SQUID-based technology. The first demonstration of a noncryogenic sensor with a SQUID-system level sensitivity (<5 fT/√Hz) was described in 2010 by Schwindt and Johnson (2010) who used optically pumped magnetometers (OPM) for registration of brain activity. OPM is a compact device consisting mainly of a laser, a photodiode, and a gas cell. The gas cell is the sensitive element of an OPM and contains vapor of one of the alkali metals K, Cs, Rb, or He.

Happer and Tang (1973) discovered spin-exchange relaxation free (SERF) mode of operation for OPMs that reduces spin-exchange intensity and allows readout of the cell's collective magnetic moment. In SERF mode, magnetometers operate at a high alkali metal vapor density and near-zero background magnetic field, which allows OPM to achieve a sensitivity of 0.16 fT/√Hz for K vapor cell (Dang, Maloof, & Romalis, 2010; Kominis, Kornack, Allred, & Romalis, 2003) comparable to SQUID systems. The theoretical limit of OPMs is currently shown to near 0.01 fT/√Hz (Ledbetter, Savukov, Acosta, Budker, & Romalis, 2008).

One of the limitations of the SERF-mode sensors is the requirement for low ambient field that is achieved using expensive magnetically shielded rooms (MSRs) and sometimes special system of coils to suppress the residual field and its gradient (Holmes et al., 2018; Iivanainen, Zetter, Grön, Hakkarainen, & Parkkonen, 2019). In 1999 W. Happer's group discovered a novel scheme that provides partial suppression of the spin-exchange relaxation rate at high pumping intensities in the nonzero field (Appelt, Ben-Amar Baranga, Young, & Happer, 1999). This approach yields high sensitivity in Earth's ambient environment and allows for shield-free registration of the magnetic fields produced by cortical sources (Limes et al., 2020).

Most of the OPMs developed to date demand heating which in turn requires on average a 5 mm thick thermal insulation layer. This precludes the sensors to be placed directly onto the scalp and increases the distance from neuronal sources to the vapor cell, the sensitive element of the sensors, and therefore reduces the SNR in the measured signals. Recent reports (Labyt et al., 2018; Morales et al., 2017) present [4]He OPMs operating at room temperature; at the moment, however, such devices have the sensitivity of about 210 fT/√Hz and allow for measuring only powerful brain sources.

The OPMs do not require cooling to cryogenic temperatures for operation and can be assembled into flexible arrays around the head, adapting to any head size and shape. This way the sensitive element of the atomic magnetometers appear located uniformly and closer to brain sources because of only a 6.5 mm distance between the vapor cell and the outer housing of the sensor. Compact implementations of SERF OPMs already resulted in several multichannel laboratory OP-MEG systems (Borna et al., 2017; Borna et al., 2020; Boto et al., 2017; Boto et al., 2018; Lin et al., 2019) that show robust operation. The 20-channel system was able to achieve high-quality response recording with standard peak recognition while showing semiquantitative similarity with SQUID recordings (Borna et al., 2020). Nowadays, the OP-MEG studies are being continued and there are several SERF OP-MEG systems in the world containing up to 50 channels (Hill et al., 2020). Noteworthy that in one of the recent development reports a 432-channel system is mentioned which was built using 48 custom-made units each containing nine vapor cells.

These developments on the forefront of OPM-based MEG systems represent a very significant step forward and hold promise to revolutionize the entire field of functional neuroimaging. The commercial availability of OPMs has launched a new era of MEG expanding into the areas traditionally occupied by EEG such as registration of encephalogram of a freely moving person (Boto et al., 2018) and measurement of brain activity outside of a laboratory setting (Limes et al., 2020; Zhang, Mhaskar, Smith, & Prouty, 2020). The new developments to come are likely to resolve the remaining issues related to low bandwidth to allow registration of the higher frequency brain activity components. However, the nonsolid nature, complexity of microfabrication, and high prices are seen as limiting factors for the broader spread of this exciting technology.

In the current article, we present the first solid-state MEG-feasible sensor that operates at room temperature according to the flux-gate principle and uses appropriately shaped yttrium-iron garnet films (Vetoshko et al., 2016a) as the sensitive element. The high-sensitivity fluxgate technology exploited in our sensor may offer a set of serious advantages over OPMs and SQUIDs in the context of MEG application. Our yttrium-iron garnet magnetometer (YIGM) is solid state, has wide dynamic range, operates at room temperature and unlike modern commercially available SERF-based OPMs does not require calibration before each use. The theoretical sensitivity of YIGM is lesser than 1 fT/√Hz, which in combination with its compact dimension and other properties make it a perfect candidate for the multichannel MEG application. In our experiments, we have observed sensitivity of about 35 fT/√Hz which is likely to be improved by the factor of 10 in the nearest future.

In what follows below, we will present the initial MEG feasibility study that uses our YIGM sensor for registering human alpha rhythm. We will also describe the basic operational principle and the initial analysis of the sensitivity and intrinsic noise properties relevant to MEG application. In order to validate our measurements, we use the OP-MEG system, which has been chosen due to comparable YIGM scalp–sensor distances.

2 | SENSOR DESCRIPTION

In general, the device operation is similar to the flux-gate type magnetometers. The magnetic core is located inside modulating coils. High sensitivity is achieved due to coherent magnetization reversal by

rotation. The magnetization vector rotation maintains a saturated state and prevents the formation of the domain walls. In our case, the magnetic core is a single-crystal ferrite-garnet epitaxial film, shaped in a special way, and the coils have orthogonal axes in order to create a rotating saturating magnetic field in the plane of the ferrite-garnet film. The special design allows to make the saturating field as low as 5 Oe and to create coherent magnetization reversal with a magnetic field rotation frequency of 100 kHz. The low saturating field was achieved by magnetic film edge geometry approximation to elliptic one by steps. The coils are pumping and probing the element at the same time. The pumping field rotates the magnetization with a constant angular speed. When the magnetization of the core is changing it reflects on the inductivity of the coils. An external field makes deviation in the angular speed of the magnetization vector, which creates subharmonics in a probe signal. The measurement signal is obtained from the second harmonic, which is typical for the flux-gate sensor type.

A single-crystal ferrite-garnet film, which was used as the core of the magnetic sensor, was produced by high-temperature liquid-phase epitaxy from a solution melt. This technology makes it possible to obtain magnetic crystals with a quality close to that of the substrate material. Our samples used high-quality single crystal GGG substrates manufactured by Saint-Gobain. In addition to a very low value of magnetic losses (Gilbert's magnetic damping constant is less than 10^{-5}), garnet ferrites obtained by this technology allow substitution of elements inside the crystal lattice, leading to a significant decrease in anisotropy fields, and, accordingly, high magnetic susceptibility (Prokopov et al., 2016; Syvorotka, Vetoshko, Skidanov, Shavrov, & Syvorotka, 2015). The combination of these two factors results in low magnetization reversal noise.

In order to conduct MEG experiments, the sensor was fixed on a massive wooden stand. The stand is placed on a damping material made of soft polymer to prevent mechanical vibrations (see Figures 1a and 3)

The linear dimensions and the arrangement of the sensitive axes of the YIGM sensor and the QuSpin OPM QZFM Gen-1/2 device are compared in Figure 1a and b, respectively. The sensitive element of the sensor is represented with a thin film with size of $38 \times 38 \times 0.01$ mm. The overall volume of the sensitive core is about 14.4 mm^3, which is comparable or lesser than typical OPM gas
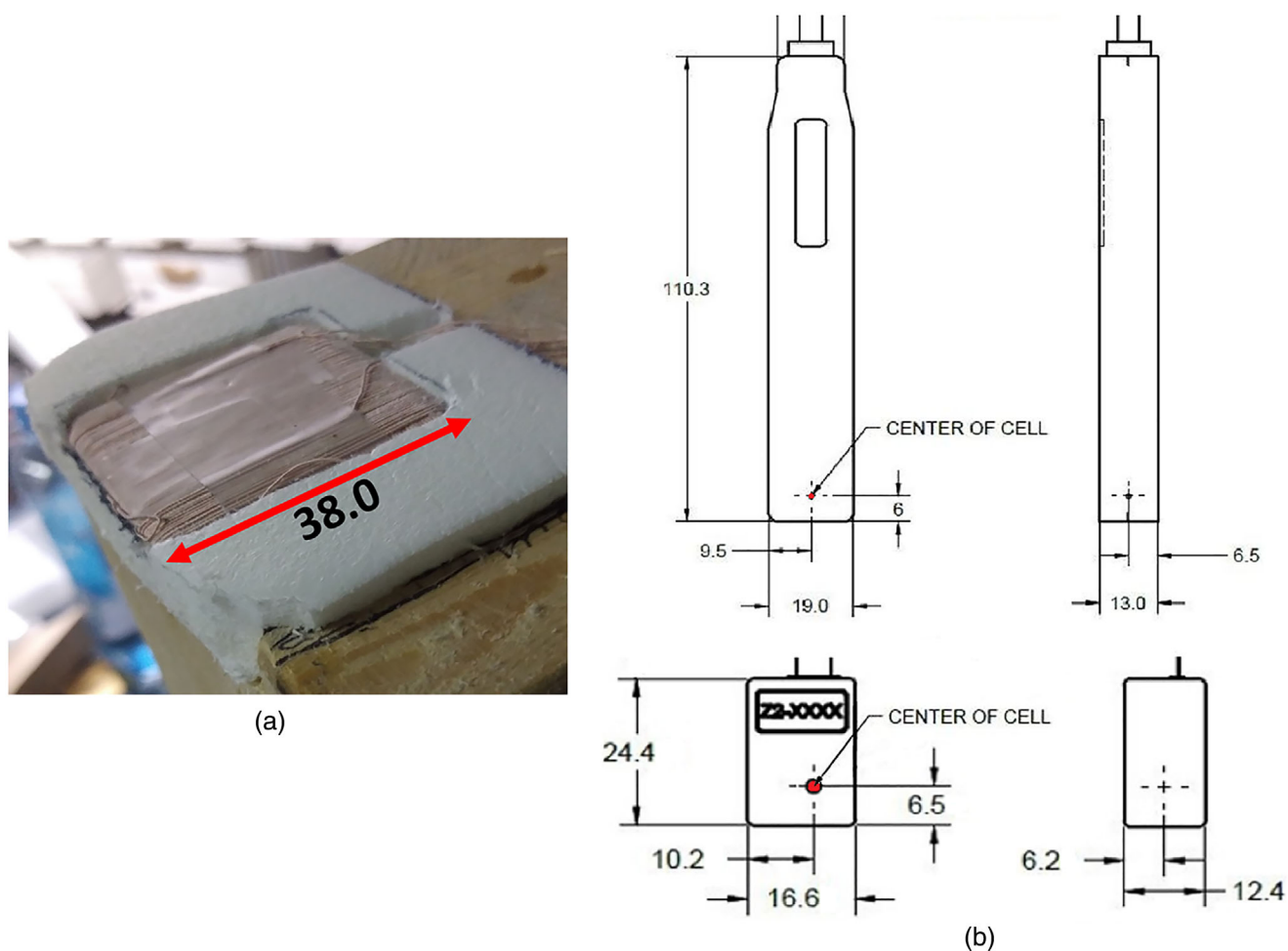

FIGURE 1 Sensor linear sizes and sensitive axes; T stands for tangential and N stands for normal field component: (a) YIGM sensitive element in winding; (b) Sensor head of OPM QZFM Gen 1.0 (top) and 2.0 (bottom) magnetometers. YIGM, yttrium-iron garnet films. Source: quspin.com

FIGURE 2 The OP-MEG system used to find locations with high magnitude of alpha waves (a) and (b); the scheme of OPM locations on the scalp (c)
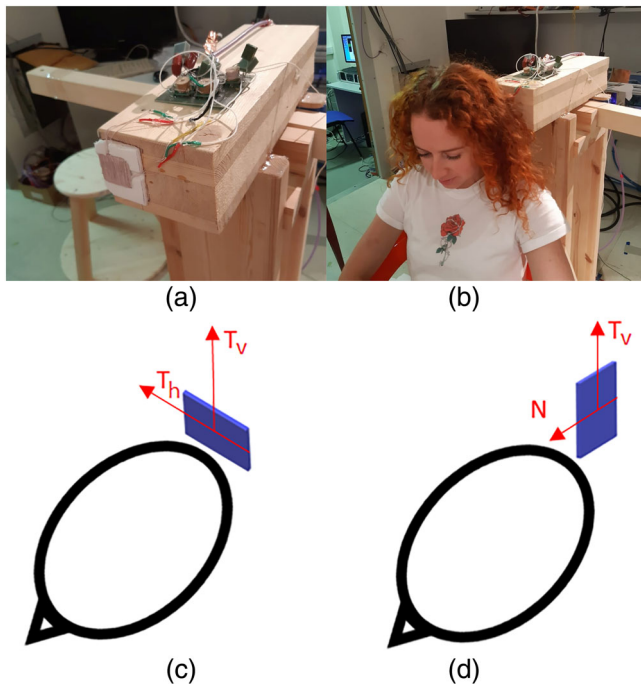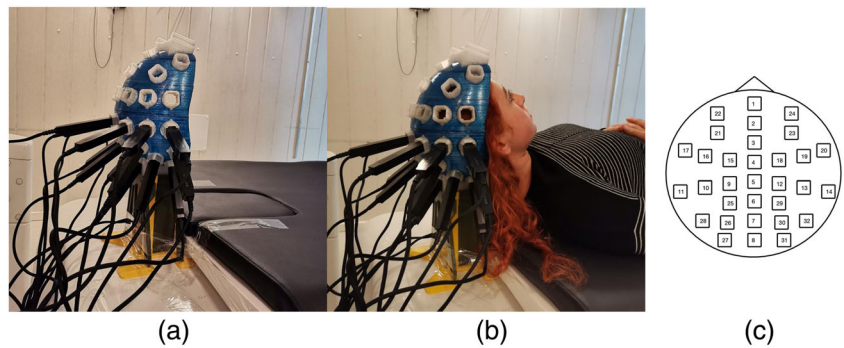

(a) (b) (c)

(a) (b)

(c) (d)

FIGURE 3 The experimental setup for alpha-rhythm registration using the YIGM: the sensor (a), subject position for alpha-rhythm registration (b); YIGM sensitive axes with respect to mutual head–sensor location: tangential displacement (c); normal displacement (d). YIGM, Yttrium-iron garnet magnetometer

cell volume. For example, volume of QuSpin QZFM gas cell is about 27 mm^3. Taking into account the thickness of the winding (1 mm per side), the overall size of YIGM is about 38 × 38 × 2 mm. Depending on the relative position according to the subject's head, the sensor can detect either two tangential or one normal and one tangential components of the magnetic field as explained later in Section 3.6.

The size of the sensor-sensitive element can be further minimized. First of all, we are planning to increase the pumping frequency, which allows to increase the sensitivity while keeping the same dimensions or to decrease size keeping the same sensitivity. For example, increasing the frequency by 10 gives us the theoretical possibility to decrease the sensitive part volume by 10. We need to note, however, that increasing pumping frequency requires more careful

and thoughtful engineering of the electronics due to additional losses in the coils, which are defined by the geometrical properties of the coil wires. Using the current geometry of sensor coils, it is possible to increase the pumping frequency up to 1–3 MHz (now it is 100 kHz). In case of further increase of frequency (higher than the limit of 3 MHz), the dissipation will grow dramatically due to concurrency between the skin and proximity phenomena. Thus, it is reasonable to increase the pumping frequency by 6–20 times in order to achieve better sensitivity. The decrease of sensor size is also possible, but we need to take into account that it leads to a change in the coil geometry, and thus demands thorough engineering. Also, the saturating field should be lower, which is planned to be achieved by more precise edge elliptical geometry approximation with steps.

3 | METHODOLOGY

In our feasibility study presented here, we have chosen to perform a comparative analysis of human alpha rhythm registered with OPM and YIGM sensors. The existence of a clear behavioral correlate, high signal amplitude, and comparative simplicity of the alpha-wave registration experiments make this rhythm a good candidate for the proof-of-concept study illustrating the feasibility of YIGM sensors for registration of brain activity. One of the most attractive features of the occipital alpha rhythm is its connection to the eye closed and eye open state of a subject, which can be used to establish the physiological relevance of the obtained measurements.

3.1 | Alpha waves

Cortical encephalographic alpha rhythm is generally regarded as the electrophysiological correlate of the awake but resting conscious state. It is the most prominent signal of the ongoing EEG/MEG to wake human subjects at rest. In the last years, the reciprocal interaction between the lateral thalamic nuclei (specific relay nuclei) and the nucleus reticularis of the thalamus has been proposed to represent the central process in modulating cortical alpha activity (Steriade, 2000; Steriade, 2001). Roland (1985) estimated the size of activated cortical areas to be comparatively big (more than 6 cm^2). The traditionally defined frequency

range of the alpha band is 8–12 Hz. However, individual variations are quite large, and the mean frequency of alpha varies as a function of age, gender, and even intelligence. It is quite low in frequency in the infant human (<7 Hz), reaches its maximum in young adulthood, and declines with age (Buzsaki, 2006).

Sources of alpha rhythms may be found concentrated mainly in the region around the Calcarine sulcus, with most sources located within 2 cm of the midline (Silva, 2002). The sources produce magnetic fields with a magnitude of 100 fT while registering with conventional SQUID-MEG. The magnitude of the alpha-induced magnetic field may reach 0.1–1 pT in dependence on experimental conditions and source-sensor distance. The first registration of magnetic field related to the alpha rhythm has been provided by Cohen (1972).

3.2 | General description of the experiments

The first-time application of a new kind of sensor requires a sophisticated validation of the obtained results. The laboratory use of the OPM-based MEG systems is well established by now. Given that the OPM sensors can be positioned with respect to the subject's head similarly to the proposed YIGM sensor, we have used the OPM-based alpha band measurement for validation of the results obtained with YIGM. We performed our experiment on the group of three healthy adults[1] (below subjects) which further contributes to the reliability of our conclusions.

The conducted experiments can be divided into several parts described in detail below. We start with the calibration of the YIGM sensor by registration of magnetic induction of known magnitude followed by the empty room noise spectrum recordings performed one after another with YIGM and the OPM sensors placed in the same place in the MSR. This allows us to compare the spectral noise profiles registered at the same location with appropriately oriented OPM and YIGM, to explore the sensor noise and distinguish it from the ambient residual field present in the MSR.

After that, we use an array of the OPMs and find the OPM position individually for each subject with the largest magnitude of the occipital alpha rhythm observed in the eye-closed condition. Then we place our YIGM at these locations and conduct the main experiment of the current article demonstrating the feasibility of human occipital alpha waves registration with solid-state YIGM sensors.

3.3 | YIGM calibration

YIGM calibration process starts by a registration of a known magnetic field at the axis of the test coil with a weak current. In order to minimize the influence of the external fields on the calibration procedure the test coil and the YIGM sensor were placed inside the demagnetized three-layer permalloy shield made of a permalloy cylinder with 300 mm radius and 700 mm length. A test coil with diameter of 120 mm was built of a single turn of the wire. The coil was connected through 240 kΩ of load resistance to the signal wave generator producing 10 mV RMS voltage

at 10 Hz. Therefore, it can be concluded that the magnetic field in the center of the coil is approximately 600 fT.

3.4 | Empty room study

The experiment pursues two main goals. The first one is to determine the location (a sweet spot) in the MSR with the minimum ambient noise and to ensure that the level of noise is suitable for our alpha-rhythm registration experiments. The second goal is to study the intrinsic noise properties of our YIG sensor. Using the OPM sensors we sampled the ambient field inside the MSR and found a sweet spot (see Section 4 for the exact values of the observed fields).

The recordings of the background magnetic field inside MSR were performed one after another with YIGM and OPM sensors placed at the discovered sweet spot location with minimal magnetic interference. The orientation of sensor-sensitive axes in both cases was identical. All subsequent measurements (registration of alpha waves) were performed at the same location with minimal interference and with the same orientation of YIGM. Also, in order to examine the intrinsic noise of the YIGM, we made the recording of noise in additional magnetic shield (permalloy cylinder described above). The shield was located at the same sweet spot inside the MSR.

3.5 | OP-MEG alpha activity registration experiment

The location and most notably orientation of an equivalent current dipole approximating the generator of the occipital alpha activity vary significantly across individuals. Therefore, we may expect that the maximum magnitude of the normal and tangential components of the magnetic field will be achieved at different locations in different subjects. Therefore, we start with registration of alpha waves using the OPMs QuSpin Zero Field Magnetometer (QZFM, QuSpin Inc., Louisville, CO). We use OPMs instead of conventional SQUID-MEG system due to the two factors. First of all, with OPMs we are able to register both normal and tangential components of magnetic induction vectors which provides a natural room for comparison of the two technologies capable of measuring the same signals. Second, the sensor–scalp distances in the OPM case are comparable to those in the YIGM case. The experimental setup and the scheme of positioning the OPMs on the scalp are depicted in Figure 2.

We registered alpha wave activity in the supine position (see Figure 2b). The recording lasted for 30 s in the eyes-open condition and for the next 30 s in the eyes-closed condition. This experiment was repeated twice with OPMs calibrated to register normal and tangential components of the magnetic field. As a result of this experiment, we obtained individual locations corresponding to the maximal magnitude of the occipital alpha rhythm in the eyes-closed condition. To do so we used the power in the 8–13 Hz band of the OPM-registered signals spectrum. Since we currently have only a single

YIGM sensor we used this individually determined location with top alpha band power to perform our YIGM-based measurements described next.

3.6 | YIG-MEG alpha activity registration experiment

This is the main experiment dedicated to the alpha waves registration with a solid-state YIGM sensor. The experimental setup we used is depicted in Figure 2b. A subject sat on a wooden chair in front of the sensor so that the YIGM sensor is as close as possible to the individually determined location over the occipital lobe, which corresponds to the maximal alpha power, (see Figure 5). As it was mentioned above (see Section 2) YIGM has two sensitive axes (horizontal and vertical) and therefore can detect both tangential and radial field components, depending on mutual position of the head and the sensor (see Figure 3).

For the purposes of this article, the vertical channel was not recorded due to the high vertical magnetic noise component in our MSR. In order to detect tangential field, the subjects were asked to sit with their head surface positioned tangentially to the YIGM sensor plane, see Figure 3a. In case of the normal field detection, the subjects were asked to rotate themselves 90° on the chair and move to a spot so that the sensor's plane was orthogonal to the local head surface (Figure 3b). Similar to the OPM-based study, we recorded each subject for 30 s with eyes-open and then eyes-closed conditions.

3.7 | Analysis of experimental data

Analysis of the obtained data (both OPM and YIGM data) has been performed using Python 3.7 and its modules (SciPy, NumPy, PyPlot, etc.). We used Welch's method to compute the amplitude spectral density (ASD) of our signals (Welch, 1967). We employed a 2.0 s long

Blackman–Harris window with no overlap to achieve a tradeoff between frequency resolution and variance in our ASD estimates. Since the sampling frequencies of both sensors were set to 1,000 Hz, this window corresponds to 2,000 points for all signals under consideration. For data filtering, we used classical one-pass order 3 IIR Butterworth bandpass filters (Bianchi & Sorrentino, 2007) as implemented in SciPy.signal module with cut-off frequencies 9–12 Hz. The mentioned parameters were selected according to the results of the individual ASDs visual analysis.

4 | RESULTS

4.1 | YIGM calibration and empty room study

The results of the calibrated signal generated by test coil inside the permalloy screen are shown in Figure 4a. Figure 4b shows the spectrograms of the signal registered in empty MSR by both YIGM and OPM QZFM. Both measurements were conducted at the same location in the MSR. The recordings of the noise in the additional permalloy shield are presented in Figure 4c.

According to Figure 4b both sensors register temperate low-frequency noise (at frequencies ~20–25 and ~35–40 Hz). In the band 40–130 Hz, the OPM shows level of noise ASD of about 10 fT/√Hz, which is close to the noise level declared for QuSpin QZFM gen.1 (Osborne, Orton, Alem, & Shah, 2018). The high-frequency noise level, registered with YIGM is about 38 fT/√Hz, which allows us to assume this value to be an intrinsic noise level of our sensor.

In order to verify the latter assumption, it is shown in Figure 4c the measurements for both kinds of sensors provided in additional magnetic shield, represented with a small permalloy cylinder and located at the sweet spot inside our MSR. From Figure 4c we can conclude that both kinds of sensors demonstrate nearly identical noise levels (27 fT/√Hz for OPMs and 35 fT√Hz for YIGM). This measurement allows us to assume the intrinsic permalloy cylinder noise is
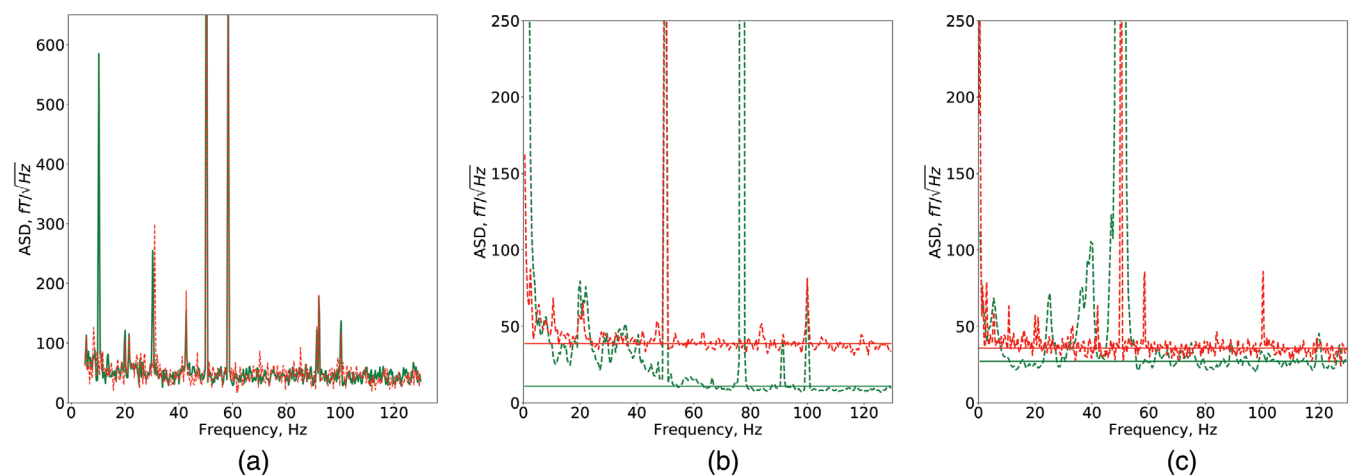

FIGURE 4 (a) Spectra of YIGM signal with the test coil turned on (green) and off (red); (b) spectra of signals of YIGM (red) and OPM (green) inside empty MSR; (c) spectra in additional shield (permalloy cylinder): YIGM—red; OPM—green. YIGM, Yttrium-iron garnet magnetometer
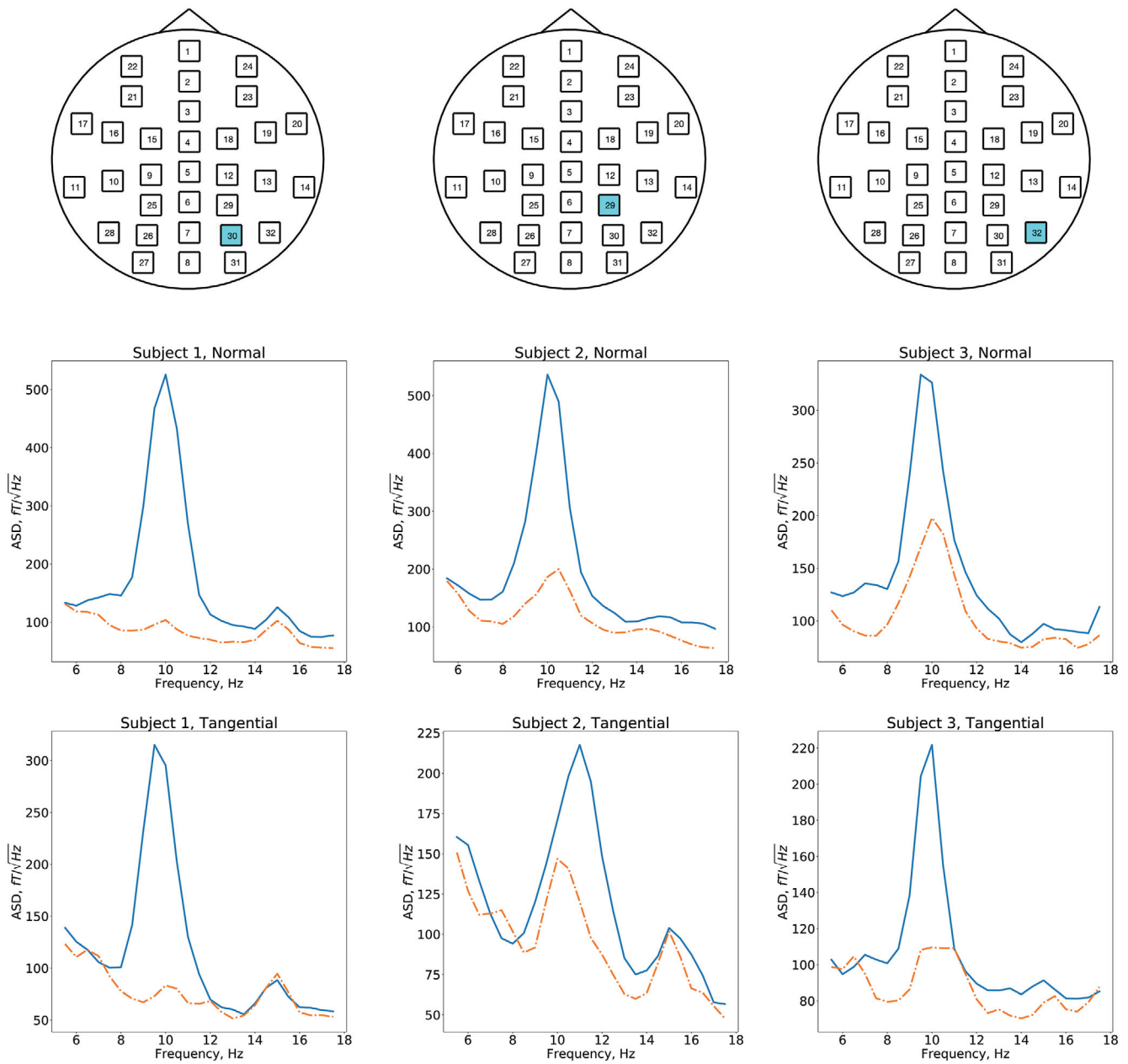
FIGURE 5 Locations of OPMs for OP-MEG alpha waves registration (top panel); middle and bottom panels—spectra of the signal measured in normal and tangential way, respectively. The spectra correspond to the OPMs marked at the top panel. Blue line—eyes closed; orange line—eyes open. OPM, Optically pumped magnetometer

about 27–30 fT/√Hz, which is lesser than 38 fT/√Hz shown by YIGM outside the screen. In this case, the intrinsic noise of YIGM is assumed to be close to the level of 35 fT/√Hz.

All three plots of Figure 4 show the very stable and independent frequency noise level for YIGM, which is about 35–38 fT/√Hz. This noise level is higher than the intrinsic noise of OPMs (35 fT/√Hz as opposed to 10 fT/√Hz for OPM, see Figure 4b). It is caused by violation of the uniform state of magnetization in the sensitive volume (garnet film) of the sensor. Main sources of this violation are

geometrical drawbacks occurring during lithography in garnet. With improvement of manufacturing process of the sensor's active body, we hope to reach the theoretical limit of sensitivity, which is lesser than 1 fT/√Hz for current size of active body and current pumping frequency (Vetoshko, Valeiko, & Nikitin, 2003).

Analysis of Figure 4b allows us to conclude that the maximum noise level registered by both sensors in the neighborhood of 10 Hz does not exceed 35 fT/√Hz. Taking into account that at a 1 cm distance from the skull the expected value of the signal produced by the

FIGURE 6 Spectra of YIGM signal measured in all subjects: top panel—normal component of the field registered along *N* sensitive axis of YIGM; bottom panel—tangential component of the field registered along T_h sensitive axis. Blue line—eyes closed; orange line—eyes opened. YIGM, Yttrium-iron garnet magnetometer
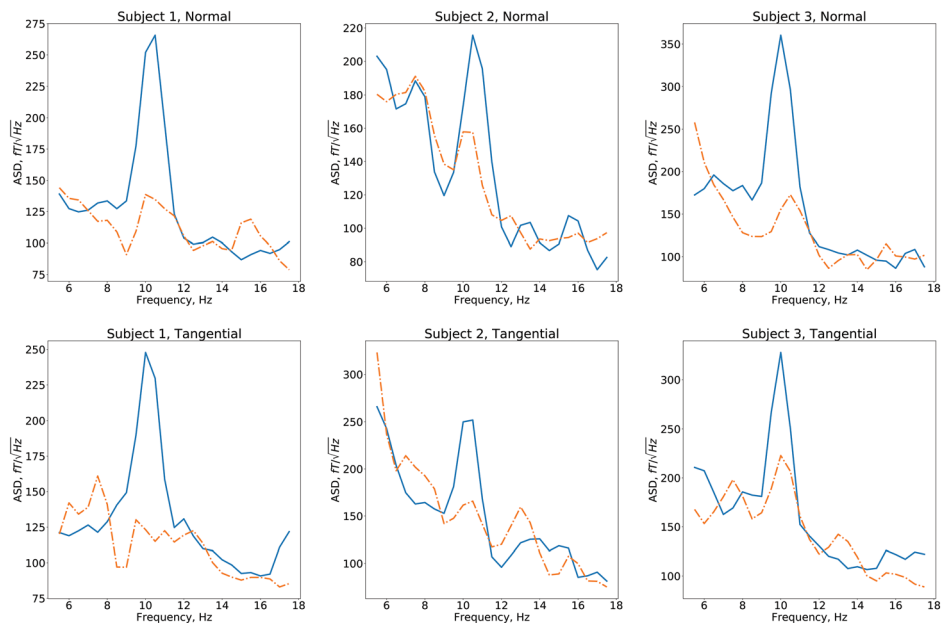
alpha rhythm is on the order of several hundred fT, we can conclude that this noise level is acceptable for the purpose of our main experiment. In the subsequent presentation, we will focus on the spectra within 5.18 Hz range for clarity reasons.

4.2 | OP-MEG alpha activity registration experiment

The purpose of the current experiment was to register alpha waves in all three subjects and to localize the areas on the scalp with the highest magnitude of the magnetic induction vector field. Such locations for each subject are shown in Figure 5 in the top line. The sensors detecting the highest amplitude of signal are highlighted with blue color. In the middle row of the figure, spectrograms of the signal, which was obtained by corresponding sensors calibrated to detect a normal component of the magnetic field, are shown. In the bottom row, the spectrograms of signals for "tangential" calibration of corresponding OPMs are presented.

4.3 | YIG-MEG alpha activity registration experiment

This experiment represents the aim of the current study—registration of alpha waves with YIGM. For this purpose, the YIGM was set into locations found during OP-MEG experiment and depicted in Figure 5 (top row). Changing the position of each subject, we registered normal and tangential components of the magnetic induction vector expecting to obtain alpha rhythm amplitudes comparable with those registered with OPMs.

Figure 6 depicts spectra of the obtained signal for each subject of the research. Spectra of the normal component are presented in the

top row of Figure 6, while the bottom row represents the tangential components.

5 | DISCUSSION

5.1 | The alpha-rhythm measurements

As we can see from the spectra above (Figures 5 and 6), frequency of alpha waves registered in all subjects falls into the 9–11 Hz range, which conforms well with the expected range for subjects of 25–35 years old tested in our experiments. In order to isolate the alpha-band oscillation in our data, we filtered the obtained YIGM signals in the 9, 11 Hz band, and superimposed the segments of this data registered during the eyes-open and eyes-closed conditions on a single graph as shown in Figure 7a–c for the three subjects. The blue and orange lines represent the signals recorded during the eyes-closed and eyes-opened conditions, respectively. We have also visualized our observations in a way similar to that used by D. Cohen in his 1972 paper heralding the use of SQUIDS for human alpha registration. In Figure 7d and e we show the normal component of the YIGM measured activity around the moment when the eyes were closed. The entire experiment duration was close to 1 min, and the subjects were asked to close their eyes after 30 s from the start of the recording. The orange line represents the envelope obtained as the absolute value of the band-filtered signal Hilbert transform.

5.2 | YIGM and OPM signals comparison

The ASDs in Figures 5 and 6 allow for a quantitative comparison of the alpha rhythm measurements obtained with OPM and YIGM. The observed ASD magnitudes appear to be comparable for both sensor
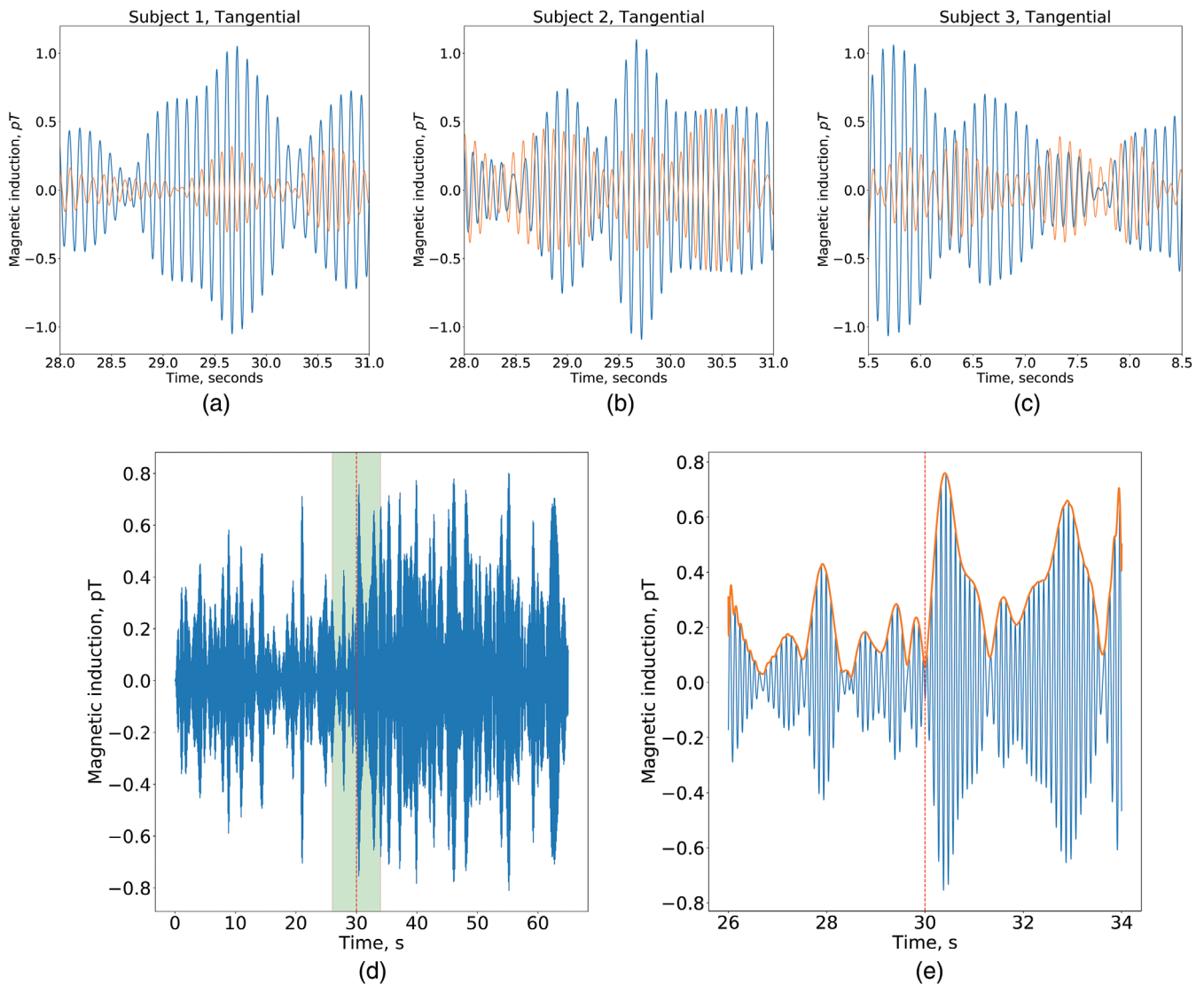
FIGURE 7 Signal of YIGM obtained during the experiment of registering the tangential component T_h filtered in band (9, 11) Hz. (a–c) Comparison of signal amplitude in band while eyes are open/close for each subject (blue line represents closed eyes). (d,e) The whole signal filtered in band (9, 11) Hz and its part bounded with a blue box around the moment of closing the eyes (red-dashed line) for subject 1, respectively. YIGM, Yttrium-iron garnet magnetometer

types. Interestingly, the second and the third subjects demonstrate a more pronounced tangential component of the alpha-rhythm when measured with YIGM compared to the OPM measurements, where we observe a relatively low magnitude of this tangential component (see Figures 5 and 6). This observation can be explained by the assessment of distances between the sensors and the hypothesized cortical alpha rhythm generator. Indeed, the OPM measurements of the normal and tangential components are characterized by one and the same distance between the vapor cell and the hypothesized alpha rhythm generator when measuring both components. In the YIGM case, the distance between the cortical source and the sensitive element depends on the mutual arrangement of the sensor with respect to the head surface (see Figure 3c and d). During the registration of the normal component, the YIGM is oriented so that its edge points toward the subject's head as shown in Figure 3d, which increases the mean

distance from the brain source to the sensitive element comparing with the sensor location when the tangential component is registered (see Figure 3c). This leads to the observed increase in the magnitude of the tangential components as measured by YIGM sensors. Using an improved setup in our follow-up studies we will investigate this phenomenon more closely as it may have serious implications for the future whole-head YIG-MEG system design.

5.3 | Discussion on sensitivity

The sensitivity of an MEG device naturally depends on two main factors: intrinsic sensor sensitivity and source-to-sensor distance. For the measurements of tangential components, YIGM array can be placed directly on the scalp, which reduces source-to-sensor distance

compared to that for SQUIDs and the commercially available OPMs. Indeed, SQUID sensors require cooling in a dewar with 2.5–3 cm thick walls, while the standard "hot" OPM's sensitive element is a vapor cell heated to around (100–120)°C which requires insulation and results in 0.6 cm separation between the proximal wall of the vapor cell and the scalp. In the future, some additional possibilities to decrease the source-to-sensor distance for OPMs can be made: better thermal isolation for "hot" OPMs, the usage of room-temperature OPMs [e.g., [4]He-based OPMs (Labyt et al., 2018; Morales et al., 2017)], and so on. Currently, however, the YIGM provides the smallest source-to-sensor distance for tangential component measurements, and comparable to OPMs source-to-sensor distance when registering normal components. Indeed, unlike OPMs and SQUIDs, the proposed solid-state YIGM sensor is flat by design (see Section 2) and operates at room temperature. When measuring the tangential component of the occipital alpha rhythm, we can place the YIGM sensitive element less than 2 mm away from the scalp, which makes it located twice as close to the hypothesized cortical source and leads to a significant SNR increase.

Such reduced scalp-to-sensor distance allows for a potentially higher sensitivity of the YIGM compared to the OPMs and SQUIDS when measuring the tangential component. Indeed, the simulation study (Iivanainen, Stenroos, & Parkkonen, 2017) shows that the source topography power is much higher for the sensors, placed several millimeters from the scalp. For example, it was shown that the topography power of OPMs located near the head surface is 5.3–7.5 times higher than that for the state-of-the-art SQUID systems. This gain is less pronounced for deep brain sources but remains 4.5–6.5 times higher than for the SQUIDs depending on the measured component orientation. Also Iivanainen et al. (2017) show much higher total information capacity of the sensor array when sensors are located closer to the head surface.

The overall sensitivity is defined by the signal-to-noise ratio and therefore depends not only on the source-to-sensor distance but also on the intrinsic sensor noise that is rather high for the current generation of YIGM and measures around 35 fT/√Hz, which is 10 times higher than that of SQUIDs. Taking advantage of the closer distance to the scalp we are still able to resolve the superficial cortical sources with our YIGM sensor, however, deeper sources remain equally difficult to detect for both SQUIDs and YIGM sensors. However, given our experience with YIGM sensors we see the potential to reduce the intrinsic noise properties by using a proper technological and manufacturing process. Theoretical limit of YIGMS was shown to be about 1 fT/√Hz (Vetoshko et al., 2003) and in our future studies, we plan to build a new generation of YIGMs by employing a more sophisticated production process and get closer to this theoretical noise floor level. We will also explore the optimal probe geometry taking advantage of the intrinsic noise properties of the new generation YIGMs.

5.4 | Multichannel YIG-MEG construction

The design of a multichannel YIG-MEG system is another major task that we plan for the nearest future. This ambitious work will require producing a number of YIGMs with similar properties, development of the sensor fixation devices and optimal probe design algorithms as well as sensor-to-head co-registration methodology. This will obviously require a detailed exploration of the mutual interference of closely located sensors.

Reassuringly, based on our previous studies, we can expect low level of cross-talk between the sensors. The YIGM considered in this publication has previously been used within the framework of bio-magnetic measurement. Detailed studies of the vector distribution of the magnetic field produced by human hearts (Gusev et al., 2017; Vetoshko et al., 2016a) and rats hearts (Vetoshko et al., 2016b) were carried out. Additionally, as a part of the magnetocardiography device development, a three-channel system with three simultaneously operating sensors has been built.

Generally, the interaction of YIGM occurs in two scenarios: (a) interaction of the pump field, (b) interaction of the response fields caused by the measured field (second harmonic). The interaction of the pumping fields of the sensors can be minimized by using a coherent (or one) sinusoidal pumping signal source. Also, it is desirable that the rotation of the vectors of neighboring sensors coincide. Small additive changes in the pump fields caused by neighboring sensors can be compensated by changing the pump field in each sensor separately. In fact, these changes are insignificant and their correction was not required when using three sensors simultaneously (Vetoshko et al., 2016a). The interaction of the response fields is minimized by the feedback system. Since the field is measured by the zero tracking method, that is, the feedback signal reduces the amplitude of the measured effect to the noise level, so much interaction is not expected and was not detected in our earlier MCG experiment.

We can consider various schemes of positioning YIGM sensors around the human head. One possible way is to simply cover the head surface with tangentially oriented sensor planes resulting in 40–50 vector magnetometers registering tangential field components. To register the radial component the magnetometers can be oriented perpendicularly to the head surface. Sensors located both tangentially and radially can also be combined. It is also possible to construct planar gradiometers based on the measurements of the pairs of nearby magnetometers. Since it is possible to further miniaturize the YIGM sensors (Vetoshko, 2017), the number of sensors in the final system may be increased. The choice of the exact configuration needs to be based on optimizing specific formal criteria such as information transfer coefficient which is going to be addressed in our upcoming reports.

The recent simulation study by Tierney et al. (2020) also may give us hints regarding the composition of the sensor array of our multichannel YIG-MEG system. For example, considering the alpha-rhythm normal component measurements, we can see the SNR of the current generation of YIGM about 10–20 dB. Taking into account that, for normal component measurement, the scalp-to-sensor distance is comparable to that of OPMs, we can conclude that we need about 90–200 channels in order to have a spatial resolution of 5 mm. Despite the fact that we seem to be able to achieve this number for normal component measurements, the measurement of deeper or shallow

sources will be impossible with the current generation of YIGMs due to the SNR that would drop to −15 or −20 dB for such sources. Assuming, however, the noise of the following generation of YIGM, for example, 15 fT/√Hz, we may obtain the SNR of ~6–10 dB for shallow sources, which will make it possible to design a 100–200 channel YIG-MEG system for studying the activity of deeper sources. With the approximation to the theoretical limit of noise for YIGM sensors (about 1 fT/√Hz), the SNR even for deeper sources may increase up to 20–40 dB (depending on the location and the dipole moment), which will allow us to achieve a 10 mm resolution for deeper sources with only 80 channels. Moreover, in case of YIGM sensors, the scalp-to-sensor distance appears to be around 2 mm, which leads to higher SNR.

5.5 | SERF-free nature

Commercially available implementations of the OPM technology (e.g., QuSpin, FieldLine) operate according to the SERF principle and therefore require a low ambient field. This imposes strict requirements on the magnitude of the ambient field and its spatial smoothness. For example, the dynamic range of the QuSpin QZFM Gen. 2.0 is ±5 nT (see, e.g., site quspin.com). Commercially available SERF mode OPMs require low (<50 nT, (Osborne et al., 2018)) ambient fields that can be achieved with costly magnetic shielding. The dynamic range of the currently used YIGM is 10 μT and further can be improved to up to 100 μT (Vetoshko, 2017), which makes it naturally operable with the Earth's magnetic field.

At the same time, OPM solutions operate according to the scheme discovered by Happer's group in 1999 with suppression of the spin-exchange relaxation rate at high pumping intensities in non-zero fields (Appelt et al., 1999). This approach yields high sensitivity in Earth's ambient environment and allows for shield-free registration of the magnetic fields produced by cortical sources (Limes et al., 2020). However, such sensors measure the total field and require additional considerations to exploit the linearity of the MEG forward modeling, an analytic approach commonly used in the interpretation of the directed field components traditionally measured with MEG sensor arrays. To this end, YIMG sensor offers natural axial sensitivity in the Earth's field and when used in a gradiometric configuration to subtract the ambient field should support the existing forward and inverse modeling approaches.

5.6 | The power consumption

The power consumption of OPM is 4.5 W, 700 mW of which are irradiated by a sensor head itself (Osborne et al., 2018). Thus, the helmet containing, for example, 50 OPMs will have power consumption of about 35–40 W. The power consumption of the whole human body will be approximately 100 W (Starner, 1996). Therefore, we can expect some discomfort and the need for cooling in the OPM-based MEG systems. In contrast, the YIGMs operate at room temperature

and consume about 100 mW (Vetoshko, 2017), which solves any problems with overheating and the subject's discomfort. Lastly, due to simplicity of construction, YIGMs are potentially cheaper compared to both OPMs and SQUIDs. YIGM does not contain parts with limited lifetime, which makes it durable and guarantees no performance deterioration.

6 | CONCLUSION

In this work, we demonstrated the possibility of using a solid-state YIGM to register brain activity according to the magneto-encephalographic principle. To show this, we designed an experiment for alpha-rhythm registration and validated our YIGM measurements with those obtained with commercially available OPMs.

It is important to emphasize that the YIGM sensor used in this experiment is the first solid-state magnetic field sensor with such a low noise level. The solid-state sensors are, in principle, easier to integrate and maintain. The device operates at room temperature, which, first of all, makes it cheaper to maintain than SQUID, and, second, allows for further reduction of the distance between the sensor and the brain source. The latter obviously depends on the shape of the sensor: flat shape allows the magnetometer to be placed right onto the head surface. The sensor implements vector measurement mode by registering magnetic field vector projections onto its surface, which results in measuring two tangential components of the magnetic field simultaneously.

Finally, according to theoretical estimations, the devices based on this technology can provide a sensitivity of about 1 fT/√Hz. This fact together with the reported observations justifies the need for further exploration of the YIGM technology and advancing it toward developing a multichannel MEG system based on the fully solid-state magnetic field sensors. Creation of such a device will be a seminal step in the MEG hardware development and will contribute to revolutionizing the entire field of noninvasive functional neuroimaging.

DATA AVAILABILITY STATEMENT
1The data that support the findings of this study are available from the corresponding author upon reasonable request.

ORCID
Nikolay Koshev 🄳 https://orcid.org/0000-0001-7241-3304

ENDNOTE
[1] The experiment was carried out in accordance with the recommendations of the Declaration of Helsinki and its amendments, and the

protocol was approved by the National Research University Higher School of Economics ethics committee. All subjects were healthy humans who gave written informed consent in accordance with the Declaration of Helsinki.

REFERENCES

Andersen, L. M., Oostenveld, R., Pfeiffer, C., Ruffieux, S., Jousmäki, V., Hamäläinen, M., ... Lundqvist, D. (2017). Similarities and differences between on-scalp and conventional in-helmet magnetoencephalography recordings. *PLoS One*, *12*(7), 1–19. https://doi.org/10.1371/journal.pone.0178602

Andersen, L. M., Pfeiffer, C., Ruffieux, S., Riaz, B., Winkler, D., Schneiderman, J. F., & Lundqvist, D. (2020). On-scalp meg squids are sensitive to early somatosensory activity unseen by conventional meg. *NeuroImage*, *221*, 117157.

Appelt, S., Ben-Amar Baranga, A., Young, A. R., & Happer, W. (1999). Light narrowing of rubidium magnetic-resonance lines in high-pressure optical-pumping cells. *Physical Review A*, *59*(3), 2078–2084. https://doi.org/10.1103/PhysRevA.59.2078

Baillet, S. (2017). Magnetoencephalography for brain electrophysiology and imaging. *Nature Neuroscience*, *20*(3), 327–339.

Bianchi, G., & Sorrentino, R. (2007). *Electronic filter simulation & design*. Boston, MA: McGraw Hill Professional.

Boon, L. I., Geraedts, V. J., Hillebrand, A., Tannemaat, M. R., Contarino, M. F., Stam, C. J., & Berendse, H. W. (2019). A systematic review of meg-based studies in parkinson's disease: The motor system and beyond. *Human Brain Mapping*, *40*(9), 2827–2848.

Borna, A., Carter, T. R., Colombo, A. P., Jau, Y.-Y., McKay, J., Weisend, M., ... Schwindt, P. D. (2020). Non-invasive functional-brain-imaging with an opm-based magnetoencephalography system. *PLoS One*, *15*(1), e0227684.

Borna, A., Carter, T. R., Goldberg, J. D., Colombo, A. P., Jau, Y.-Y., Berry, C., ... Schwindt, P. D. (2017). A 20-channel magnetoencephalography system based on optically pumped magnetometers. *Physics in Medicine & Biology*, *62*(23), 8909.

Boto, E., Holmes, N., Leggett, J., Roberts, G., Shah, V., Meyer, S. S., et al. (2018). Moving magnetoencephalography towards real-world applications with a wearable system. *Nature*, *555*(7698), 657–661.

Boto, E., Meyer, S. S., Shah, V., Alem, O., Knappe, S., Kruger, P., et al. (2017). A new generation of magnetoencephalography: Room temperature measurements using optically-pumped magnetometers. *NeuroImage*, *149*, 404–414.

Buzsaki, G. (2006). *Rhythms of the brain*. Oxford, England: Oxford University Press.

Cohen, D. (1972). Magnetoencephalography: Detection of the brain's electrical activity with a superconducting magnetometer. *Science*, *175*(4022), 664–666.

da Silva, F. L. (2013). Eeg and meg: Relevance to neuroscience. *Neuron*, *80*(5), 1112–1128.

Dang, H., Maloof, A. C., & Romalis, M. V. (2010). Ultrahigh sensitivity magnetic field and magnetization measurements with an atomic magnetometer. *Applied Physics Letters*, *97*(15), 151110.

Faley, M., Dammers, J., Maslennikov, Y., Schneiderman, J., Winkler, D., Koshelets, V., ... Dunin-Borkowski, R. (2017). High-tc squid biomagnetometers. *Superconductor Science and Technology*, *30*(8), 083001.

Gusev, N., Vetoshko, P., Kuzmichev, A., Chepurnova, D., Samoilova, E., Zvezdin, A., ... Belotelov, V. (2017). Ultra-sensitive vector magnetometer for magnetocardiographic mapping. *Biomedical Engineering*, *51*(3), 157–161.

Happer, W., & Tang, H. (1973). Spin-exchange shift and narrowing of magnetic resonance lines in optically pumped alkali vapors. *Physical Review Letters*, *31*(5), 273.

Hari, R., & Salmelin, R. (2012). Magnetoencephalography: From squids to neuroscience: Neuroimage 20th anniversary special edition. *NeuroImage*, *61*(2), 386–396.

Hill, R. M., Boto, E., Rea, M., Holmes, N., Leggett, J., Coles, L. A., ... Brookes, M. J. (2020). Multi-channel whole-head opm-meg: Helmet design and a comparison with a conventional system. *NeuroImage*, *219*, 116995. https://doi.org/10.1016/j.neuroimage.2020.116995

Holmes, N., Leggett, J., Boto, E., Roberts, G., Hill, R. M., Tierney, T. M., ... Bowtell, R. (2018). A bi-planar coil system for nulling background magnetic fields in scalp mounted magnetoencephalography. *NeuroImage*, *181*, 760–774.

Iivanainen, J., Stenroos, M., & Parkkonen, L. (2017). Measuring meg closer to the brain: Per- formance of on-scalp sensor arrays. *NeuroImage*, *147*, 542–553.

Iivanainen, J., Zetter, R., Grön, M., Hakkarainen, K., & Parkkonen, L. (2019). On-scalp meg system utilizing an actively shielded array of optically-pumped magnetometers. *NeuroImage*, *194*, 244–258.

Kominis, I., Kornack, T., Allred, J., & Romalis, M. V. (2003). A subfemtotesla multichannel atomic magnetometer. *Nature*, *422*(6932), 596–599.

Koptelova, A., Bikmullina, R., Medvedovsky, M., Novikova, S., Golovteev, A., Grinenko, O., et al. (2018). Ictal and interictal meg in pediatric patients with tuberous sclerosis and drug resistant epilepsy. *Epilepsy Research*, *140*, 162–165.

Labyt, E., Corsi, M.-C., Fourcault, W., Laloy, A. P., Bertrand, F., Lenouvel, F., ... Morales, S. (2018). Magnetoencephalography with optically pumped 4 he magnetometers at ambient temperature. *IEEE Transactions on Medical Imaging*, *38*(1), 90–98.

Ledbetter, M., Savukov, I., Acosta, V., Budker, D., & Romalis, M. (2008). Spin-exchange-relaxation-free magnetometry with Cs vapor. *Physical Review A*, *77*(3), 033408.

Limes, M., Foley, E., Kornack, T., Caliga, S., McBride, S., Braun, A., ... Romalis, M. (2020). Portable magnetometry for detection of biomagnetism in ambient environments. *Physical Review Applied*, *14*(1), 011002.

Lin, C.-H., Tierney, T. M., Holmes, N., Boto, E., Leggett, J., Bestmann, S., ... Miall, R. C. (2019). Using optically pumped magnetometers to measure magnetoencephalographic signals in the human cerebellum. *The Journal of Physiology*, *597*(16), 4309–4324.

Mandal, P. K., Banerjee, A., Tripathi, M., & Sharma, A. (2018). A comprehensive review of magnetoencephalography (meg) studies for brain functionality in healthy aging and alzheimer's disease (ad). *Frontiers in Computational Neuroscience*, *12*, 60.

Morales, S., Corsi, M., Fourcault, W., Bertrand, F., Cauffet, G., Gobbo, C., et al. (2017). Magnetocardiography measurements with 4he vector optically pumped magnetometers at room temperature. *Physics in Medicine & Biology*, *62*(18), 7267.

Osborne, J., Orton, J., Alem, O., & Shah, V. (2018). Fully integrated standalone zero field optically pumped magnetometer for biomagnetism. In *Steep dispersion engineering and opto-atomic precision metrology XI* (Vol. 10548, p. 105481G). International Society for Optics and Photonics.

Prokopov, A., Vetoshko, P., Shumilov, A., Shaposhnikov, A., Kuz'michev, A., Koshlyakova, N., ... Zvezdin, V. B. (2016). Epitaxial bi–gd–sc iron-garnet films for magnetophotonic applications. *Journal of Alloys and Compounds*, *671*, 403–407.

Pulvermüller, F., Shtyrov, Y., & Ilmoniemi, R. (2003). Spatiotemporal dynamics of neural language processing: An meg study using minimum-norm current estimates. *NeuroImage*, *20*(2), 1020–1025.

Roland, P. (1985). Cortical organization of voluntary behavior in man. *Human Neurobiology*, *4*(3), 155–167.

Schwindt, P. D., & Johnson, C. N. (2010). Atomic magnetometer for human magnetoencephalography, Sandia Report SAND2010-8443.

Silva, F. H. D. (2002). Electrical potentials. In *Encyclopedia of the human brain* (pp. 147–167). San Diego, CA: Academic Press.

Starner, T. (1996). Human-powered wearable computing. *IBM Systems Journal*, *35*(3.4), 618–629.

Steriade, M. (2000). Corticothalamic resonance, states of vigilance and mentation. *Neuroscience*, *101*(2), 243–276.

Steriade, M. (2001). Impact of network activities on neuronal properties in corticothalamic systems. *Journal of Neurophysiology*, *86*(1), 1–39.

Syvorotka, I. I., Vetoshko, P. M., Skidanov, V. A., Shavrov, V. G., & Syvorotka, I. M. (2015). In-plane transverse susceptibility of (111)-oriented iron garnet films. *IEEE Transactions on Magnetics*, *51*(1), 1–3.

Tierney, T. M., Mellor, S., O'Neill, G. C., Holmes, N., Boto, E., Roberts, G., et al. (2020). Pragmatic spatial sampling for wearable meg arrays. *Scientific Reports*, *10*(1), 1–11.

Vetoshko, P. (2017). *Remagnetization of iron-garnet films by coherent rotation for sensitive elements of magnetic sensors (in Russian)*. (Ph.D. thesis). M.N. Mikheev Institute of Metal Physics of the Ural Branch of the Russian Academy of Sciences (IMP UB RAS).

Vetoshko, P., Gusev, N., Chepurnova, D., Samoilova, E., Syvorotka, I., Syvorotka, I., … Belotelov, V. (2016a). Flux-gate magnetic field sensor based on yttrium iron garnet films for magnetocardiography investigations. *Technical Physics Letters*, *42*(8), 860–864.

Vetoshko, P., Gusev, N., Chepurnova, D., Samoilova, E., Zvezdin, A., Korotaeva, A., & Belotelov, V. (2016b). Rat magnetocardiography using a flux-gate sensor based on iron garnet films. *Biomedical Engineering*, *50*(4), 237–240.

Vetoshko, P. M., Valeiko, M. V., & Nikitin, P. I. (2003). Epitaxial yttrium iron garnet film as an active medium of an even-harmonic magnetic field transducer. *Sensors and Actuators A: Physical*, *106*(1–3), 270–273.

Welch, P. (1967). The use of fast Fourier transform for the estimation of power spectra: A method based on time averaging over short, modified periodograms. *IEEE Transactions on Audio and Electroacoustics*, *15*(2), 70–73. https://doi.org/10.1109/TAU.1967.1161901

Zhang, R., Mhaskar, R., Smith, K., & Prouty, M. (2020). Portable intrinsic gradiometer for ultra-sensitive detection of magnetic gradient in unshielded environment. *Applied Physics Letters*, *116*(14), 143501.